The Astrophysical Journal, 794:78 (7pp), 2014 October 10 doi:10.1088/0004-637X/794/1/78

INITIATION OF CORONAL MASS EJECTION EVENT OBSERVED ON 2010 NOVEMBER 3: MULTI-WAVELENGTH PERSPECTIVE

Sargam Mulay[1], Srividya Subramanian[1], Durgesh Tripathi[1], Hiroaki Isobe[2], and Lindsay Glesener[3]
[1] Inter-University Centre for Astronomy and Astrophysics, Post Bag-4, Ganeshkhind, Pune 411007, India
[2] Center for the Promotion of Interdisciplinary Education and Research, Kyoto University, Kyoto 606-8501, Japan
[3] Space Sciences Laboratory, University of California at Berkeley, 7 Gauss Way, Berkeley, CA 94720, USA
Received 2014 January 4; accepted 2014 July 21; published 2014 September 25

ABSTRACT

One of the major unsolved problems in solar physics is that of coronal mass ejection (CME) initiation. In this paper, we have studied the initiation of a flare-associated CME that occurred on 2010 November 3 using multi-wavelength observations recorded by the Atmospheric Imaging Assembly on board the *Solar Dynamics Observatory* and the *Reuven Ramaty High Energy Solar Spectroscopic Imager*. We report an observation of an inflow structure initially in the 304 Å and the 1600 Å images a few seconds later. This inflow structure was detected as one of the legs of the CME. We also observed a non-thermal compact source concurrent and near co-spatial with the brightening and movement of the inflow structure. The appearance of this compact non-thermal source, brightening, and movement of the inflow structure and the subsequent outward movement of the CME structure in the corona led us to conclude that the CME initiation was caused by magnetic reconnection.

Key words: Sun: atmosphere – Sun: corona – Sun: coronal mass ejections (CMEs) – Sun: filaments, prominences – Sun: transition region – Sun: UV radiation

Online-only material: animation, color figures

1. INTRODUCTION

Coronal mass ejections (CMEs) are the most energetic Solar events. These are considered to be the direct consequence of dynamics of the solar atmosphere. CMEs are one of the fundamental processes responsible for the transfer of mass and energy from the Sun into the heliosphere. They represent potential threats to space weather and the geo-space climate. In spite of considerable advancement in the quality of the observational data and numerical simulations, the initiation of CMEs is still a matter of strong debate. For reviews, see, e.g., Schwenn et al. (2006), Gopalswamy et al. (2006), and Webb & Howard (2012).

Observationally, the evolution of CMEs has been found to mainly have three different stages, namely, initiation, acceleration, and propagation. The initiation phase, also called the slow rise phase, is often found to be associated with the pre-flare phase of the associated soft X-ray flaring emission (e.g., Chifor et al. 2006), while the acceleration phase of the CME often corresponds to magnetohydrodynamic instability and the main phase or impulsive phase of the flare and the propagation phase of the CME corresponds to the decay phase of the flare (see, e.g., Zhang & Dere 2006; Chifor et al. 2006, 2007; Tripathi et al. 2013 and references therein).

Magnetic reconnection (Parker 1963; Petscheck 1964) has been considered to play an important role in the initiation of almost all dynamic and eruptive solar events, such as CMEs (Sterling & Moore 2005; Chifor et al. 2006, 2007), flares (see, e.g., Sweet 1958; Shibata 1996; Priest & Forbes 2002; Tripathi et al. 2004; Su et al. 2013), the partial eruption of prominences (Gibson & Fan 2006; Tripathi et al. 2006a, 2006b, 2009, 2013), coronal jets (Shibata et al. 1992, 1994; Shibata 2008; Chifor et al. 2008), etc., observed in the solar atmosphere. There has been much indirect evidence for the reconnection phenomena such as reconnection inflow (Yokoyama et al. 2001; Narukage & Shibata 2006; Savage et al. 2012; Takasao et al. 2012) and outflow (McKenzie & Hudson 1999, 2001; Tripathi et al. 2006b, 2007; Savage et al. 2010) and non-thermal hard X-ray (HXR) sources associated with the initiation of CMEs (Chifor et al. 2006). However, these different signatures have been observed individually in separate dynamic events. CMEs are almost always associated with solar flares, for which reconnection is a very important concept (Benz et al. 2008).

A flare-associated CME was observed on 2010 November 3 originating from the partially occulted active region AR 11121. This event was well observed by the Atmospheric Imaging Assembly (AIA) on board the *Solar Dynamics Observatory* (*SDO*), the Reuven Ramaty High Energy Solar Spectroscopic Imager (*RHESSI*), and radio instruments. A number of papers have been published addressing various issues associated with flares and CMEs. For example, the evolution phase of the CME and its associated flare is studied by Cheng et al. (2012), Reeves & Golub (2011), Savage et al. (2012), Kumar, Innes (2013), Foullon et al. (2011), Cheng et al. (2011), Hannah, Kontar (2013), and Glesener et al. (2013) including the relationship between flares and CMEs. The associated decimetric/metric type II radio burst is analyzed by Bain et al. (2012) and Zimovets et al. (2012). Moreover, this event showed the first evidence of magnetic Kelvin–Helmholtz instability in the solar corona which was reported by Foullon et al. (2011, 2013). However, none of the above papers studied the near-limb region of the event or considered the initiation phase of the CME.

The main aim of this paper is to study the initiation of this flare-CME event by making use of the multi-wavelength observations recorded by AIA/*SDO* and *RHESSI*. By combining these observations, we find that magnetic reconnection causes the initiation of this CME event. AIA images taken at 304 Å and 1600 Å show that the signature of the inflow structure is consistent with the time and location of HXR emission imaged by *RHESSI*. The rest of the paper is structured as follows.

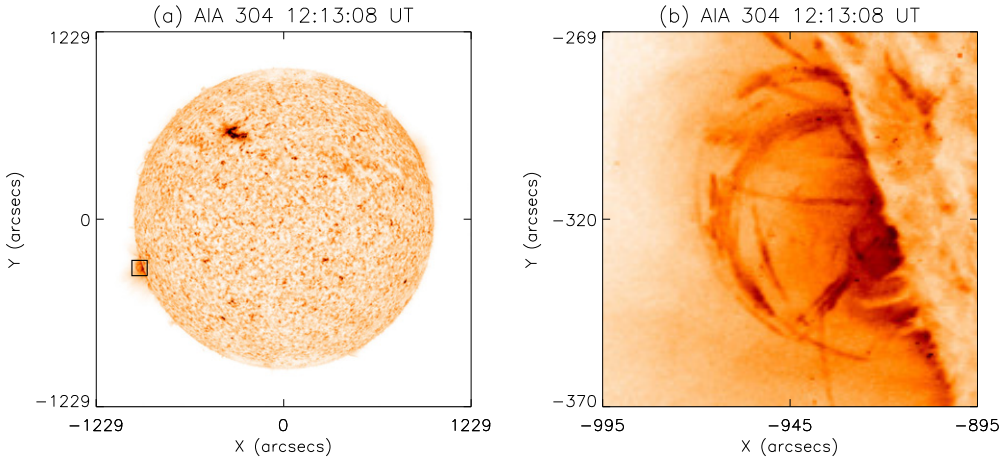

Figure 1. Left panel: full disk image of the Sun at 304 Å. The overplotted box shows the region where the CME eruption took place. Right panel: 304 Å image corresponding to the overplotted box shown in the left panel.

(A color version of this figure is available in the online journal.)

In Section 2, we report the observations. In Section 3, we describe our data analysis and results, and follow with a discussion and conclusions in Section 4.

2. OBSERVATIONS

In the current analysis, we have focused on AIA and *RHESSI* data obtained during the early rise phase of the CME initiation. The AIA (Lemen et al. 2012) on board *SDO* provides continuous full disk observations of the solar atmosphere in 10 different UV/EUV passbands with a high spatial resolution (pixel size of 0.″6), a temporal resolution of 12 s, and a field of view covering up to 1.3 solar radii. We have concentrated only on three AIA channels, namely 1600 Å, dominated by C IV emission (transition region temperature and the continuum emission from the photosphere), 304 Å, dominated by chromospheric He II at quiet conditions, and 131 Å, dominated by coronal Fe VIII, Fe XX, and Fe XXIII. We refer to O'Dwyer et al. (2010) and Del Zanna et al. (2011) for a detailed description of the EUV filters in AIA and their temperature response. The observations recorded using other wavelength channels have been extensively analyzed by previous authors. The features studied in the current paper have not been observed in other wavelength channels. All the data are reduced and prepared using the standard procedures available in the solarsoft libraries.

The *RHESSI* mission (Lin et al. 2002) provides high-resolution spectra and images in HXRs, from 3 keV to 17 MeV. It has nine sub-collimators, all with different spatial resolutions and each sub-collimator does not modulate flux from sources larger than its resolution (Hurford et al. 2002). In this work, we have used only sub-collimators 3–5 which have resolutions from 7 to 20 arcsec.

On 2010 November 3, AIA observed an event originating from the east limb at around 12:13 UT. The source region was located 5°–7° behind the optical limb (Glesener et al. 2013). The source region appeared on the visible disk on 2010 November 5 and was called AR 11121. The left panel of Figure 1 displays the full disk image of the Sun taken using the 304 Å filter. The small box overplotted on the east limb represents the 100″ × 100″ area of interest. The right panel shows the close up view of the region shown via box in the left panel. Figure 2 shows 3 s averaged soft X-ray flux of the associated C4.9 class flare between 1 and 8 Å obtained using the *GOES* 14 satellite. The profile suggest that the flare started at around 12:07 UT with a peak at around 12:21 UT. A pre-flare bump is also noticeable before the main phase of the flare.

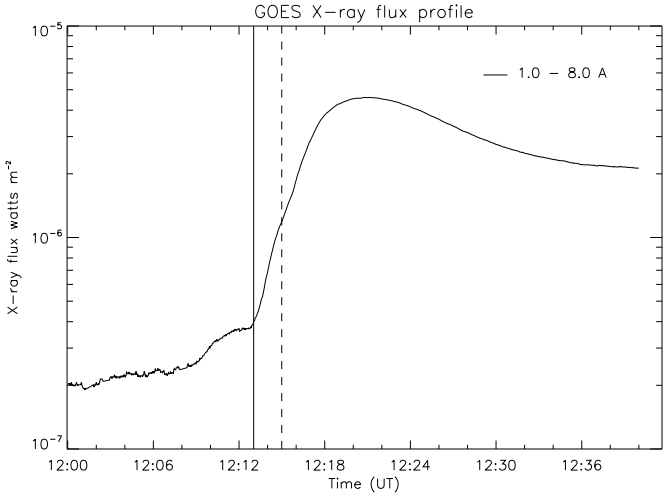

Figure 2. Integrated soft X-ray flux (1–8 Å) observed by the *GOES* 14 satellite on 2010 November 3. The continuous vertical line shows the beginning of the event at about 12:13:08 UT and the dotted vertical line marks the end at about 12:15:20 UT, when the 304 Å inflow loop disappears completely.

Figure 3 displays the complete evolution of the flare-CME event. A bright loop-like structure emanates from the source region at 12:13:09 UT, which later became a CME. With passing time, the structure evolves into a flux rope with a current sheet underneath. The box overplotted shows the region that we analyze in detail.

3. DATA ANALYSIS AND RESULTS

Figure 4 shows observations of the source region taken with the 304 Å (top row) and 1600 Å (bottom row) filters between 12:13 and 12:17 UT, which corresponds to the rise phase during the CME initiation and the impulsive phase of the associated flare (see Figure 2). The field of view of these images corresponds to the boxes shown in Figures 1 and 3. The images in both wavelengths show loop-like structures and other filamentary structures. A close analysis of images taken in 304 Å (top row) reveals a pre-existing vertical structure (with respect to the limb; marked with arrows in the first and second panels of Figure 4), that moves southward, as seen in the

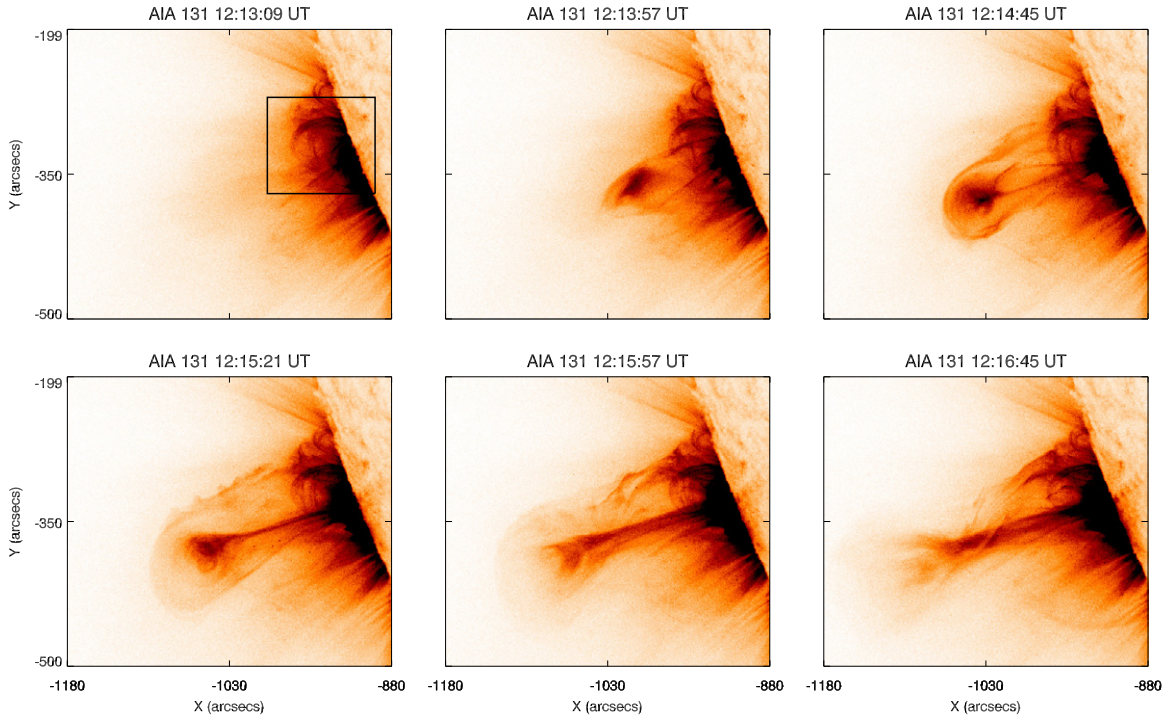

Figure 3. Sequence of images taken using the 131 Å filter showing the complete evolution of the CME event. The box in the top left panel shows the field of view which is analyzed in detail.

(A color version of this figure is available in the online journal.)

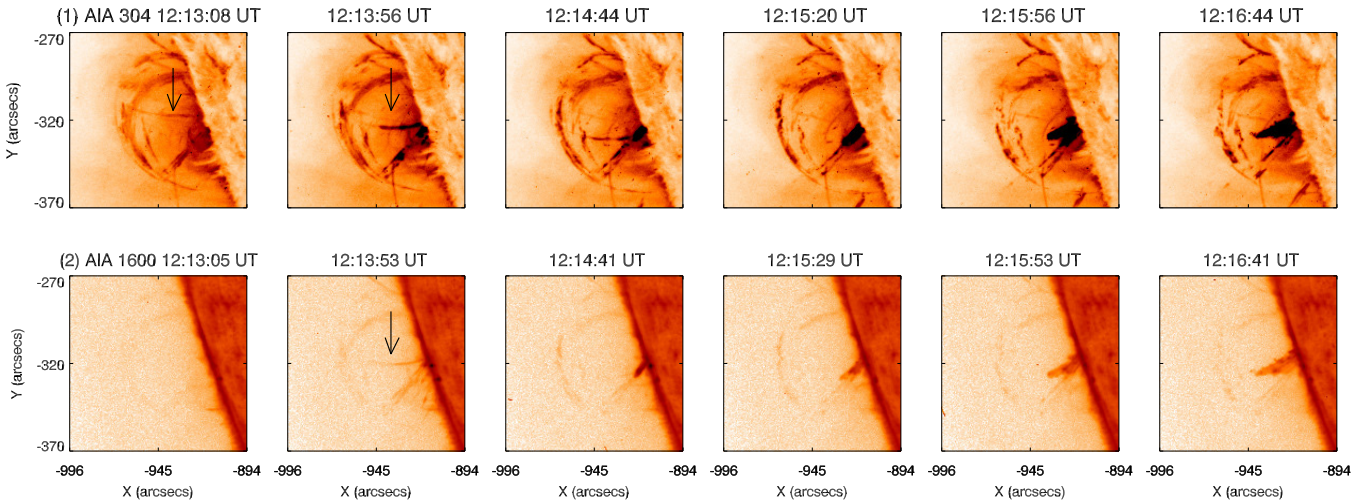

Figure 4. Sequence of images during the impulsive acceleration phase of the CME, at 304 Å (first row) and 1600 Å (second row). The FOV of these images corresponds to the box shown in Figure 3.

(A color version of this figure is available in the online journal.)

subsequent images. We refer to this structure as the "inflow structure" hereafter. The vertical inflow structure first brightens in the 304 Å image at 12:12:56 UT. With passing time, as it moves southward, it becomes brighter and finally disappears at 12:15:20 UT. By tracking a point on the inflow structure at different instances of time until it disappears, we determined a speed of 105 km s^{-1}.

This inflow structure remains invisible in the 1600 Å images until the structure starts moving in the 304 Å images. Once the inflow structure starts to move south and brightens in 304 Å, it becomes visible in the 1600 Å images at about 12:13:28 UT (the structure is shown by an arrow in the second panel of the bottom row in Figure 4). This structure is, however, seen until 12:14:17 UT in 1600 Å images and disappears completely, which coincides with the fading of this structure in the 304 Å images. A jet-like outward moving structure, similar to that is seen in the 304 Å images, is also observed. The absence of this structure in the 1700 Å images confirms that the 1600 Å emission mainly comes from the C IV, i.e., the emitted plasma is at the transition region temperature.

Figure 5 shows three snapshots of composite images simultaneously recorded using 304 Å (green) and 131 Å (red). The arrow in the left panel indicates the inflow structure seen in the 304 Å images (discussed earlier). The middle panel shows the inflow structure seen in 304 Å connected to the northern leg of the blob seen in 131 Å, as marked by an arrow. The arrow in

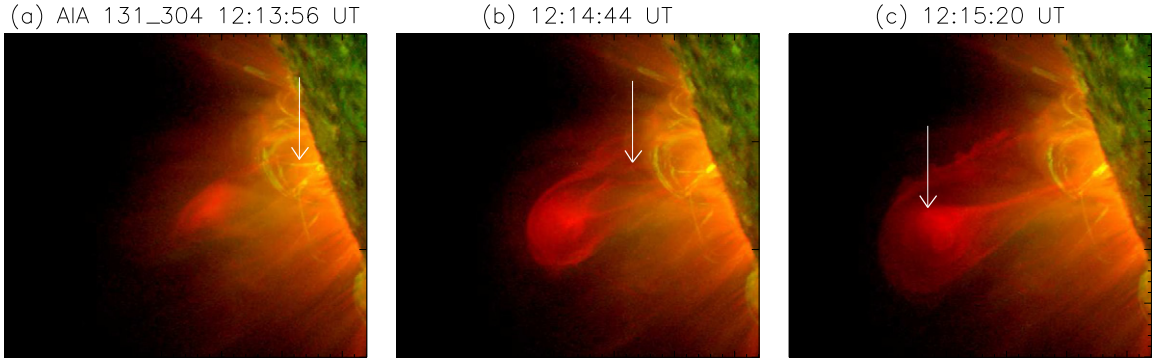

Figure 5. Composite images of observations recorded in 304 Å (green) and 131 Å (red). The arrow in the left panel shows the inflow structure seen in 304 Å and that in the middle panel shows the connection between the inflow structure and the northern leg of the flux rope. The arrow in the right panel shows the fully formed flux rope structure.

(A color version and an animation of this figure are available in the online journal.)

the right panel shows the fully formed flux-rope-like structure. The associated animation (composite SUBSCRIPTNBmovie SUBSCRIPTNB131 SUBSCRIPTNB304.mpg) reveals the evolution of the CME seen in 131 Å and the inflow structure seen in 304 Å. The composite animation shows a large-scale faint disturbance which occurs in close association with the first brightening of the inflow structure in the 304 Å images. A diffuse blob-like structure appears and starts to move outward in concurrence with the inflow structure sweeping in toward the south. The composite images taken at 12:14:20 UT show a blob-like structure with two legs emanating from the location where the inflow structure merges with another pre-existing structure. By 12:14:44 UT, the blob-like structure takes the shape of a fully formed flux-rope with an overlying loop. We interpret this inflow structure to be reconnection inflow, which moves south to the reconnection location at which it merges with other magnetic structures and disappears.

Distinct HXR emission regions were observed by *RHESSI* (see Figure 3 in Glesener et al. 2013). Using 18–40 keV *RHESSI* observations with the two-step CLEAN method (Krucker et al. 2011), they observed two distinct HXR sources: a compact source near the limb and a coronal extended diffuse source. The later was co-spatial and co-temporal to the main phase of the flares and the associated erupting CME as observed in the AIA 131 Å images. However, the compact source appeared about 30 s prior to the coronal extended diffuse source. The delay could not be explained by the difference in electron densities due to the much shorter time for thermalization of the accelerated electrons. An explanation could be that there were two different reconnection events, one occurring closer to the limb and another at higher altitude in the corona. The start time and location of the compact source near the limb matches the brightening and movement of the inflow structure observed in the 304 Å images shown in Figure 4. In this paper, we have therefore focused on this particular source.

Figure 6 shows the *GOES* soft X-ray flux profile integrated between 1 and 8 Å (top panel) and the HXR light curve integrated between 18 and 40 keV (bottom panel). At the beginning of the impulsive phase of the flare, an enhancement in HXR source is seen. The first appearance of this HXR emission is at 12:12:56 UT. This also marks the onset of the rise phase of CME initiation and the brightening and movement of the 304 Å inflow structure. Moreover, the HXR light curve shows two peaks (bottom panel of Figure 6). The first peak corresponds to the very early times of the impulsive phase of the flare and the intensity is about 20% larger than the second peak. The two vertical lines mark the time interval that corresponds to the brightening, movement, and disappearance of the inflow structure seen in 304 Å. In order to probe the spatial relation between the location of the near limb compact HXR source and the inflow structure observed in the 304 Å images, we have created HXR images with the CLEAN algorithm (Hurford et al. 2002). Figure 7 shows the sequence of the (reverse colored) images observed during the course of this event in 304 Å with *RHESSI* contours overplotted. The contours in each frame correspond to the ratios of the HXR fluxes observed in that particular frame with respect to the peak flux. The top middle panel corresponds to the peak timing of the HXR light curve. Hence, it shows a range of contours corresponding to 30%, 50%, 70%, and 90% of the peak flux, respectively. The box overplotted in the top-left panel shows the field of view that is used to generate the light curve of the near limb compact HXR source shown in Figure 6. As can be seen from Figures 6 and 7, the HXR emission in 18–40 keV is co-temporal with the inflow motion and co-spatial with the base of the inflow structure, suggesting that this inflow is indeed the reconnection inflow that energizes the flare. One puzzling point in this interpretation is the brightening of the inflow seen in 304 Å (Figure 7), because the inflow should be pre-heated plasma. One possibility is that the inflow is heated by the leakage of the heat from the reconnection region by thermal conduction, as suggested by Yokoyama & Shibata (1997) and Chen et al. (1999).

We have also performed the spectral analysis of the near-limb HXR source during the time interval 12:12:56–12:13:50 UT. The images were individually checked to ensure that the Clean components were not found high in the corona to verify that the images are not contaminated by flux from the high coronal source. A photon spectrum was fit to the fluxes of these Clean images for this time interval and is shown in Figure 8; fit components included a thermal distribution ($T = 21.7$ MK) and a broken power law with a spectral index of 4.2. The existence of a power-law component above 20 keV confirms a population of flare-accelerated electrons in the near-limb source. This analysis suggests the non-thermal nature of the source, demonstrating magnetic reconnection processes in action, which in turn leads to the movement of the inflow structure seen in the 304 Å observations and in the initiation of the CME event.

Figure 9 depicts the complete evolution of the initiation phase of the event. The top left panel shows the structures in the source region (shown in red), including the inflow structure (marked with a blue arrow) seen in the 304 Å image before the CME eruption. The structure depicted by blue line indicates the flux

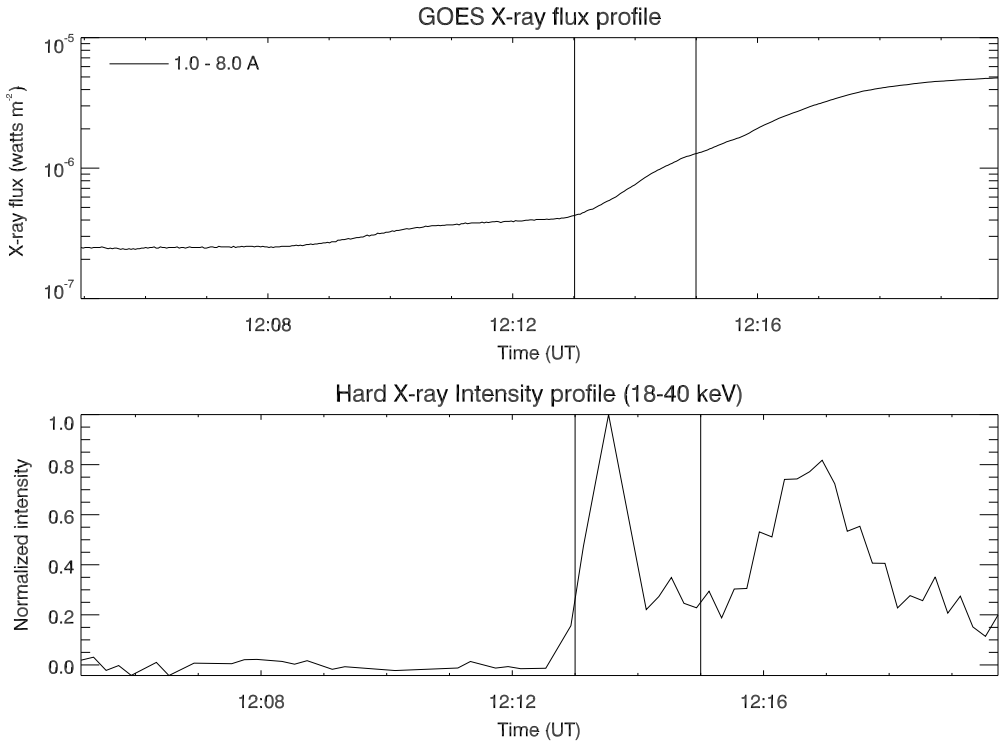

Figure 6. Top panel: *GOES* soft X-ray profile integrated between 1 and 8 Å. Bottom panel: *RHESSI* light curve between 18 and 40 keV. The two vertical lines mark the time interval that corresponds to the brightening, movement, and disappearance of the inflow structure seen in 304 Å.

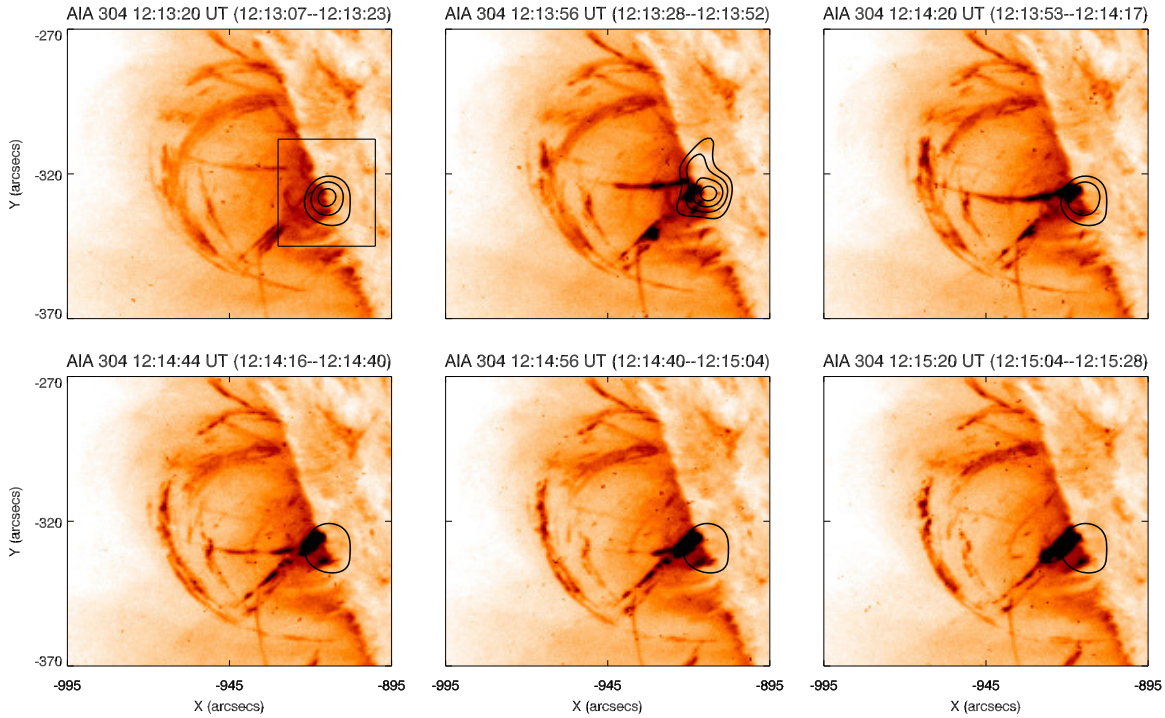

Figure 7. Sequence of images observed during the rise phase of CME initiation at 304 Å (color inverted), with *RHESSI* contours overplotted in the 18–40 keV energy band. The contours in each frame correspond to the ratio of the hard X-ray (HXR) flux observed in that particular frame with respect to the peak flux observed in the whole event (Figure 6: bottom panel). The top middle panel corresponds to the peak of the HXR light curve. The contours are 30%, 50%, 70%, and 90% of the maximum flux in the top middle image. The respective *RHESSI* images are created by combining the fine subcollimators (3, 4, and 5) with the CLEAN algorithm over the time given in the bracket. The box overplotted in the top left panel shows the field of view that is used to generate the time profile of the near limb compact HXR source.

(A color version of this figure is available in the online journal.)

rope structure as observed in 131 Å. The inflow structure in the top left panel brightens with the occurrence of a non-thermal bright compact HXR source (18–40 keV) shown in green and marked with a black arrow, observed at 12:12:56 UT. Top right panel shows the inflow structure as it appears in 304 Å and is connected to the northern leg of the blob seen in 131 Å, as marked by an arrow. The fully formed flux rope structure shown in bottom left panel and marked with an arrow later

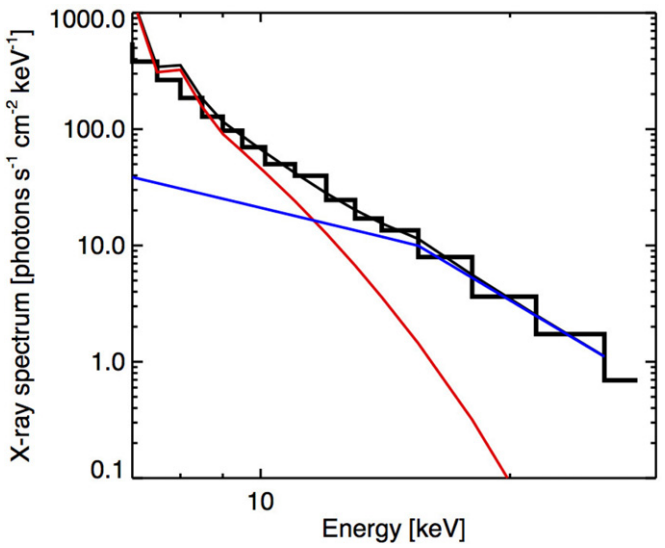

Figure 8. Hard X-ray spectrum averaged over 12:12:56–12:13:50 UT shown in black. The observations are fitted with a thermal distribution in red ($T = 21.7$ MK, EM $= 6.5 \times 10^{46}$ cm^{-3}) and a broken power law in blue (power-law index is 4.2).

(A color version of this figure is available in the online journal.)

erupts as a CME. The bottom right panel shows the evolution of jet material (shown in green) that appears concurrent with the pinching of the inflow structure. The appearance of this compact non-thermal source, brightening, and movement of the inflow structure and the subsequent outward movement of the CME structure in the corona led us to conclude that magnetic reconnection is the cause for the CME initiation. Based on the location of the HXR source followed by the moving inflow structure and subsequent UV brightening associated with the jet, we infer that the reconnection region is located at an even lower altitude than that reported by Savage et al. (2012).

4. SUMMARY AND CONCLUSIONS

The problem of CME initiation is one of the major unsolved problems in Solar physics. This has a profound impact on space weather forecasting. In this paper, we have probed the initiation phase of a well observed flare-associated CME event that occurred on 2010 November 3 using multi-wavelength observations recorded using AIA on board *SDO* and *RHESSI*. The later evolution phase of the CME and its associated flare event has been studied in detail by various authors (e.g., Reeves & Golub 2011; Savage et al. 2012; Kumar, Innes 2013; Foullon

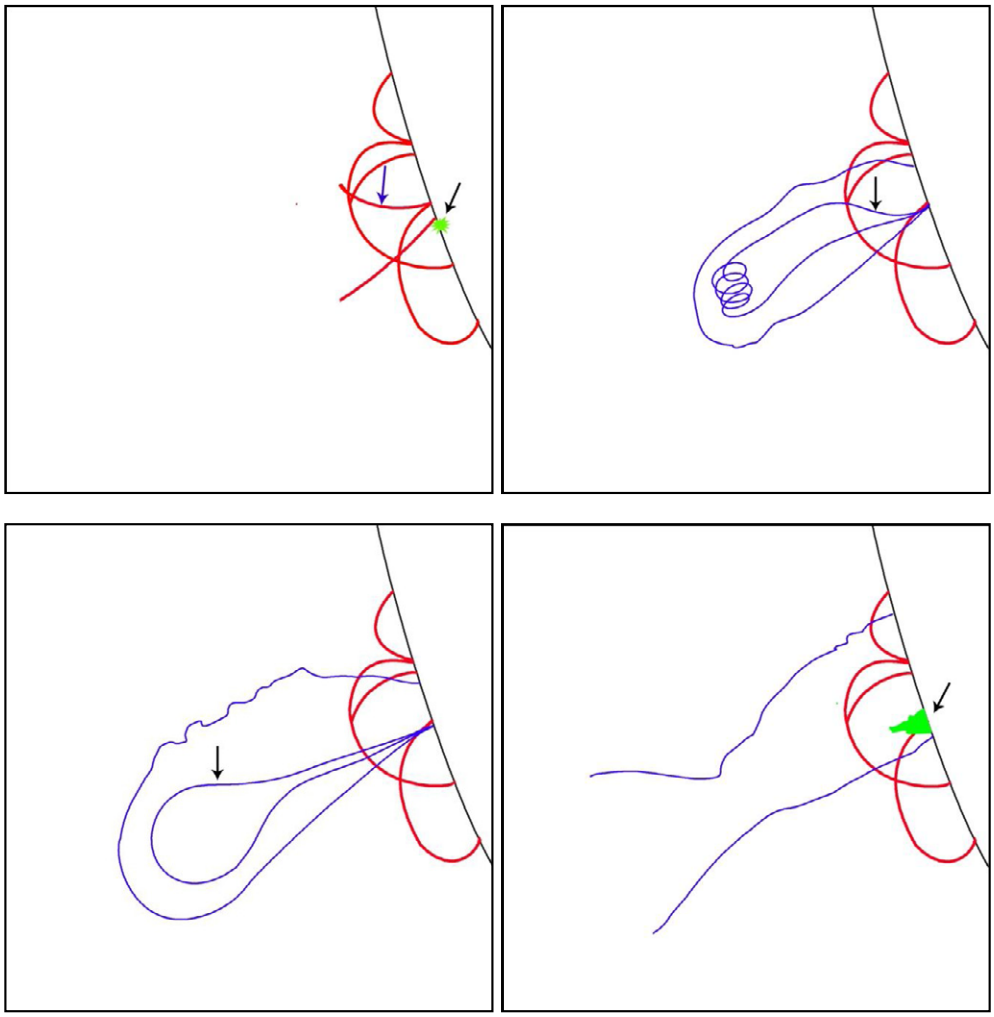

Figure 9. Schematic depiction of the complete evolution of the flare-CME event observed over the east limb. Top left panel: scenario before the event and the onset of HXR source (green and marked by an arrow) over the limb. The structure marked with the blue arrow is the inflow structure. Top right panel: inflow structure connected to the northern leg of the blob during the rise phase of CME initiation. Bottom left panel: fully formed flux rope structure with a current sheet underneath and an overlying loop structure. Bottom right panel: a jet-like (green) outward moving structure similar to that seen in the 304 Å images.

(A color version of this figure is available in the online journal.)

et al. 2011; Cheng et al. 2011; White & Verwichte (2012); White et al. (2012); Bain et al. 2012; Zimovets et al. 2012; Hannah, Kontar 2013; Glesener et al. 2013). However, no one has studied the initiation phase of the CME, which is the aim of this paper.

The results are summarized below.

1. An inflow structure was observed in the 304 Å images. The same inflow structure appeared after about a few seconds in the 1600 Å images, suggesting heating of the inflow structure, which is also demonstrated by the increase in the brightening of the inflow structure in the 304 Å observations.
2. A bubble-like structure, which later became a flux-rope-like structure and erupted as CME, started to rise in the 131 Å images exactly at the time when the inflow structure was first seen.
3. A compact HXR source was seen over the limb at about 12:12:56 UT, exactly at the time of the first brightening in the inflow structure followed by its movement. The start of the movement of the inflow structure and the appearance of the HXR compact source matched the time of the rising blob, which later manifested as a CME. The light curve of this source reveals that the HXR fluxes increase until peaking at about 12:13:30 UT, then fading to a minimum by 12:14:20 UT. The spectral analysis of the source suggests the non-thermal nature of the source, demonstrating the magnetic reconnection processes to be responsible for the HXR emission.

These observations suggest that the initiation of the CME is triggered by magnetic reconnection taking place in the source region. This is demonstrated by the brightening of the inflow structures co-temporal with the non-thermal compact HXR source in the source region and outward movement of the blob-like structure which later manifests itself as a CME.

A plausible interpretation could be the following. As it is revealed by the images obtained at 131 Å, there is a blob-like structure pre-existing in the corona with the inflow structure 304 Å as one of the legs. This structure is in stable configuration under the Lorentz force balance. Due to the evolution of the magnetic field in the source region, magnetic reconnection takes place, producing the compact non-thermal HXR. This could also be produced by magnetic reconnection between the emerging flux with pre-existing flux (Chen & Shibata 2000; Feynman & Martin 1995; Chifor et al. 2007). The magnetic reconnection would in turn change the force balance by reducing the pressure at the reconnection location. Due to this reduced pressure, the inflow structure, which is seen as one of the legs of the CME, starts to move south toward the reconnection region and eventually also reconnects and disappears. Later on, a jet-like structure emanates from the location where the inflow structure reconnects. The jet-like structure is clearly observed in the 304 Å and 1600 Å images. The detection of the HXR source, the southward movement of the inflow structure, and the rise of the CME structure in the corona are closely related to each other.

In the beginning of the event, the CME structure appears blob-like, which later revealed a helical structure with an overlying structure. Therefore, the current observation also signifies that the formation of the flux rope is likely to be a consequence of the reconnection. Moreover, for the first time, we observe signature of magnetic reconnection in lines like 304 Å and 1600 Å. Such observations may have the potential to provide information on reconnection processes occurring in partially ionized plasmas.

We thank the referee for the comments. S.M. and D.T. acknowledge support from DST under the Fast Track Scheme (SERB/F/3369/2012/2013). The AIA data are courtesy of *SDO* (NASA) and the AIA consortium. H.I. is supported by the Grant-in-Aid for Young Scientists (B, 22740121). *RHESSI* work is supported by NASA contract NAS 5-98033.

REFERENCES

Bain, H. M., Krucker, S., Glesener, L., & Lin, R. P. 2012, ApJ, 750, 44B
Benz, A. O. 2008, LRSP, 5, 1
Chen, P. F., Fang, C., Tang, Y. H., & Ding, M. D. 1999, ApJ, 513, 516
Chen, P. F., & Shibata, K. 2000, ApJ, 545, 524
Cheng, X., Zhang, J., Liu, Y., & Ding, M. D. 2011, ApJL, 732, L25
Cheng, X., Zhang, J., Saar, S. H., & Ding, M. D. 2012, ApJ, 761, 62C
Chifor, C., Mason, H. E., Tripathi, D., Isobe, H., & Asai, A. 2006, A&A, 458, 965
Chifor, C., Tripathi, D., Mason, H. E., & Dennis, B. R. 2007, A&A, 472, 967
Chifor, C., Young, P. R., Isobe, H., et al. 2008, A&A, 481, 57
Del Zanna, G., O'Dwyer, B., & Mason, H. E. 2011, A&A, 535, 46
Feynman, J., & Martin, S. F. 1995, JGR, 100, 3355
Foullon, C., Verwichte, E., Nakariakov, V. M., Nykyri, K., & Farrugia, C. J. 2011, ApJL, 729, L8
Foullon, C., Verwichte, E., Nykyri, K., Aschwanden, M., & Hannah, I. 2011, ApJ, 767, 170
Gibson, S. E., & Fan, Y. 2006, ApJL, 637, L65
Glesener, L., Krucker, S., Bain, H. M., & Lin, R. P. 2013, ApJL, 779, L29
Gopalswamy, N., Mikić, Z., Maia, D., et al. 2006, SSRv, 123, 303
Hannah, I. G., & Kontar, E. P. 2013, A&A, 553A, 10H
Hurford, G. J., Schmahl, E. J., Schwartz, R. A., et al. 2002, SoPh, 210, 61
Kumar, P., & Innes, D. E. 2013, SoPh, 288, 255
Krucker, S., Kontar, E. P., Christe, S., Glesener, L., & Lin, R. P. 2011, ApJ, 742, 82
Lemen, J. R., Title, A. M., Akin, D. J., et al. 2012, SoPh, 275, 17L
Lin, R. P., Dennis, B. R., Hurford, G. J., et al. 2002, SoPh, 210, 3
McKenzie, D. E., & Hudson, H. S. 1999, ApJ, 519, 93M
McKenzie, D. E., & Hudson, H. S. 2001, EP&S, 53, 577M
Narukage, N., & Shibata, K. 2006, ApJ, 637, 1122N
O'Dwyer, B., Del Zanna, G., Mason, H. E., Weber, M. A., & Tripathi, D. 2010, A&A, 521, 21
Parker, E. N. 1963, ApJS, 8, 177P
Petschek, H. E. 1964, BAAS, 50, 425
Priest, E. R., & Forbes, T. G. 2002, A&ARv, 10, 313P
Reeves, K. K., & Golub, L. 2011, ApJL, 727, L52
Savage, S. L., Holman, G., Reeves, K. K., et al. 2012, ApJ, 754, 13S
Savage, S. L., McKenzie, D. E., Reeves, K. K., Forbes, T. G., & Longcope, D. W. 2010, ApJ, 722, 329S
Schwenn, R., Raymond, J. C., Alexander, D., et al. 2006, SSRv, 123, 127
Shibata, K. 1996, AdSpR, 17, 9S
Shibata, K. 2008, in 37th COSPAR Scientific Assembly, 2858S
Shibata, K., Ishido, Y., Acton, L. W., et al. 1992, PASJ, 44L, 173S
Shibata, K., Nitta, N., Strong, K. T., et al. 1994, ApJL, 431, L51
Sterling, A. C., & Moore, R. L. 2005, ApJ, 613, 1221
Su, Y., Veronig, A. M., Holman, B. R., et al. 2013, NatPh, 9, 489
Sweet, P. A. 1958, in IAU Symp. 6, Electromagnetic Phenomena in Cosmical Physics, ed. Bo Lehnert (Cambridge: Cambridge Univ. Press), 123
Takasao, S., Asai, A., Isobe, H., & Shibata, K. 2012, ApJL, 745, L6
Tripathi, D., Bothmer, V., & Cremades, H. 2004, A&A, 422, 337
Tripathi, D., Gibson, S. E., Qiu, J., et al. 2009, A&A, 498, 295
Tripathi, D., Isobe, H., & Mason, H. E. 2006a, A&A, 453, 1111
Tripathi, D., Reeves, K., Gibson, S. E., Srivastava, A. K., & Joshi, N. C. 2013, ApJ, 778, 142
Tripathi, D., Solanki, S. K., Mason, H. E., & Webb, D. F. 2007, A&A, 472, 633T
Tripathi, D., Solanki, S. K., Schwenn, R., et al. 2006b, A&A, 449, 369
Wedd, D. F., & Howard, T. A. 2012, LRSP, 9, 3
White, R. S., & Verwichte, E. 2012, A&A, 537, A49
White, R. S., Verwichte, E., & Foullon, C. 2012, A&A, 545, A129
Yokoyama, T., Akita, K., Morimoto, T., Inoue, K., & Newmark, J. 2001, ApJL, 546, L69
Yokoyama, T., & Shibata, K. 1997, ApJL, 474, L61
Zhang, J., & Dere, K. P. 2006, ApJ, 649, 1100
Zimovets, I., Vilmer, N., Chian, A. C.-L., Sharykin, I., & Struminsky, A. 2012, A&A, 547, A6